Photoinduced Charge Separation and Charge Recombination in [60]Fullerene−Ethylcarbazole and [60]Fullerene−Triphenylamines in Polar Solvents

He-Ping Zeng,*,† Tingting Wang,† Atula S. D. Sandanayaka,‡ Yasuyuki Araki,‡ and Osamu Ito*,‡

Institute of Functional Molecular, South China University of Technology, Guangzhou 510641, People's Republic of China, and Institute of Multidisciplinary Research for Advanced Materials, Tohoku University, Katahira 2-1-1, Aoba-ku, Sendai 980-8577, Japan

Received: February 22, 2005; In Final Form: April 1, 2005

Molecules of C_{60} covalently connected with *N*-ethylcarbazole (EtCz) and triphenylamine (TPA) have been synthesized. Photoinduced electron transfer in C_{60}−EtCz and C_{60}−TPA has been studied in polar and nonpolar solvents using time-resolved transient absorption and fluorescence measurements. From the fluorescence lifetimes, the excited singlet state of the C_{60} moiety ($^1C_{60}$*) of C_{60}−TPA generates predominantly $C_{60}^{\bullet-}$−$TPA^{\bullet+}$, which decays quickly to the ground state within 6 ns even in polar solvents. In the case of C_{60}−EtCz, on the other hand, about half of the $^1C_{60}$* moiety generates short-lived $C_{60}^{\bullet-}$−$EtCz^{\bullet+}$, while the other half of the $^1C_{60}$* moiety is transferred to the $^3C_{60}$* moiety via intersystem crossing in dimethylformamide, in which the energy level of $C_{60}^{\bullet-}$−$EtCz^{\bullet+}$ is lower than that of $^3C_{60}$*. Thus, the charge separation takes place via $^3C_{60}$* generating $C_{60}^{\bullet-}$−$EtCz^{\bullet+}$, having a lifetime as long as 300 ns, probably because of the triplet spin character of $C_{60}^{\bullet-}$−$EtCz^{\bullet+}$. A special property of the EtCz moiety to stabilize the hole in the charge-separated state was revealed.

Introduction

During the past 15 years, many interesting fullerene derivatives have been synthesized and developed to be remarkable building blocks for the design of new photochemical molecular devices.[1−9] Fullerenes have been known as excellent electron acceptors due to their unique π-electron system, excited-state electronic properties, small reorganization energy, and absorption spectra extending to most of the visible region.[1−9] Therefore, much research on the covalently bond donor−fullerene molecules has been reported about photoinduced electron transfer to form the radical anion (electron) of the C_{60} moiety and the radical cation (hole) of the electron donor.[1−9] The efficiencies and rates of the electron-transfer processes in the donor−C_{60} molecules can be tuned by the energy of the donor−C_{60} pair, in addition to the distances and orientations between the electron-donor and C_{60} moieties.[1−9] Thus, efficient charge separation (CS) and slow charge recombination (CR) have been achieved for the donor−C_{60} molecules, serving as appropriate artificial photosynthetic models. A number of fullerene-based dyads and triads containing olefins,[10] aromatic amines,[11−14] porphyrins,[15,16] phthalocyanines,[17,18] ruthenium complexes,[19a,b] ferrocenes,[19c,20] tetrathiafulvalenes,[21,22] and oligothiophenes[23,24] as electron donors were synthesized. In these dyads and triads, the importance of the sensitizing donors and acceptors, from which the CS process takes place generating the radial cation and radical anion, has been revealed. Among the donors, aromatic amines are the most fundamental donors. Thus, various C_{60}−amine dyads with various connecting bonds have been synthesized and their photophysical properties have been investigated extensively.[11−14] In our previous papers,[25] the bridges connecting the C_{60} moiety with the donor molecules play an important role in assisting the electron-transfer ability and hole delocalization. Furthermore, in the C_{60}−amine mixture systems, photoinduced electron transfer mainly occurs via the excited triplet state of C_{60} ($^3C_{60}$*), producing long-lived radical ions, when the amine concentrations are properly low in polar solvents.[26,27] On the other hand, under high amine concentrations, the photoinduced electron-transfer process mainly occurs via the excited singlet state of C_{60} ($^1C_{60}$*), producing short-lived radical ion pairs ($C_{60}^{\bullet-}$−$amine^{\bullet+}$) in nonpolar solvents.[28]

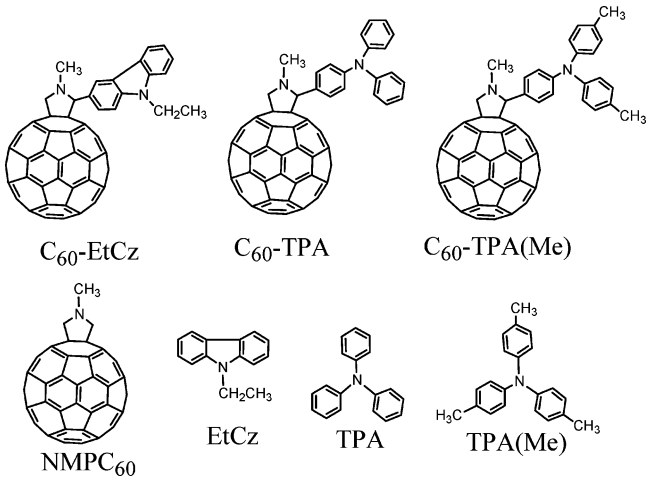

Figure 1. Molecular structures of C_{60}−TPA, C_{60}−TPA(Me), C_{60}−EtCz, and reference compounds.

In the present study, we have synthesized three dyad molecules, C_{60}−EtCz, C_{60}−TPA, and C_{60}−TPA(Me), in which C_{60} and amine donors are covalently bonded with short linkage, as shown in Figure 1. Our aim of the present study is to reveal

* Corresponding authors. E-mail: ito@tagen.tohoku.ac.jp (O.I.); zenghp@scnu.edu.cn (H.-P.Z.).
† South China University of Technology.
‡ Tohoku University.

10.1021/jp050914d CCC: $30.25
Published on Web 05/06/2005

SCHEME 1: Synthetic Route

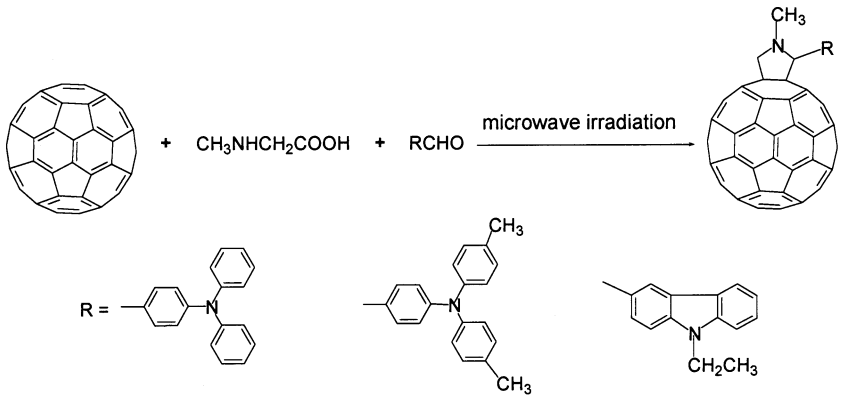

directly the CS process by measuring the rates and efficiencies of the CS processes with time-resolved fluorescence measurements with changing solvent polarity. The nanosecond lifetimes of the CS states were also evaluated by transient spectra measurements. Hence, a comparison of photoinduced electron-transfer processes between C_{60}−EtCz and C_{60}−TPA would provide valuable information about CS and CR processes of short linkage fullerene−amine donor dyads.

Results and Discussion

Synthesis. C_{60}−EtCz, C_{60}−TPA, and C_{60}−TPA(Me) and its reference compound $NMPC_{60}$ were prepared by the Prato reaction under microwave irradiation as shown in Scheme 1.[29] C_{60}−EtCz, C_{60}−TPA, and C_{60}−TPA(Me) were identified on the basis of spectroscopic methods and elemental analytical data (see Experimental Section).

Molecular Orbital Calculations. To gain insights into the molecular geometries and electronic structures of C_{60}−EtCz, C_{60}−TPA, and C_{60}−TPA(Me), molecular orbital (MO) calculations were performed using the density functional B3LYP/3-21G(*) method. The geometric parameters of the compounds were obtained after completing energy minimization. The optimized structures are shown in Figure 2. The center-to-center distances (R_{cc}) between the C_{60} moiety and the EtCz, TPA, and TPA(Me) moieties were estimated to be 9, 11, and 10 Å, respectively, from the optimized structures.

Furthermore, Figure 2 shows the spatial electron densities of the highest occupied molecular orbital (HOMO) and lowest unoccupied molecular orbital (LUMO) for C_{60}−EtCz, C_{60}−TPA, and C_{60}−TPA(Me). For the three dyads, the majority of the electron density of the HOMO was found to be located on the aromatic amine moiety, while the LUMO is localized on the C_{60} spheroid. These findings suggest that in the charge-separated state the anion radical is localized on the C_{60} spheroid, while the radical cation is localized on the aromatic amine moiety. It is interesting to note here that the calculated LUMO−HOMO gap in C_{60}−EtCz, C_{60}−TPA, and C_{60}−TPA(Me) is 1.81, 1.93, and 1.32 eV, respectively, in agreement with the electrochemically observed differences between the oxidation potential (E_{ox}) and reduction potential (E_{red}).

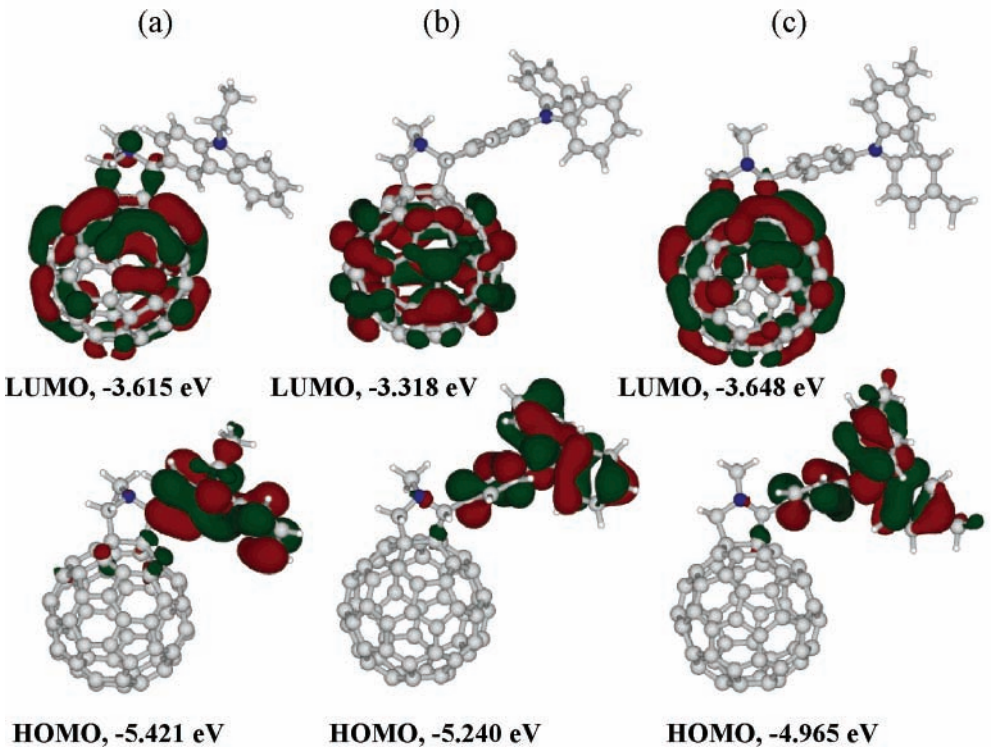

Figure 2. Optimized structures and electron densities of LUMOs and HOMOs of (a) C_{60}−EtCz, (b) C_{60}−TPA, and (c) C_{60}−TPA(Me) calculated at B3LYP/3-21G(*)+1 level.

TABLE 1: Oxidation (E_{ox}) and Reduction (E_{red}) Potentials and Center-to-Center Distances of C_{60} and Amines (R_{cc}) for C_{60}−EtCz, C_{60}−TPA, and C_{60}−TPA(Me) vs Fc/Fc^+ in PhCN

compound	solvent	E_{ox}/V	E_{red}/V	$(E_{ox} - E_{red})$/V	R_{cc}[a]/Å
C_{60}−EtCz	PhCN	0.53	−1.00	1.53	9
C_{60}−EtCz	DMF	0.41	−0.88	1.29	
C_{60}−TPA	PhCN	0.55	−1.03	1.58	11
C_{60}−TPA	DMF	0.54	−0.86	1.40	
C_{60}−TPA(Me)	PhCN	0.47	−1.01	1.48	10
C_{60}−TPA(Me)	DMF	0.40	−0.93	1.33	

[a] From optimized structures.

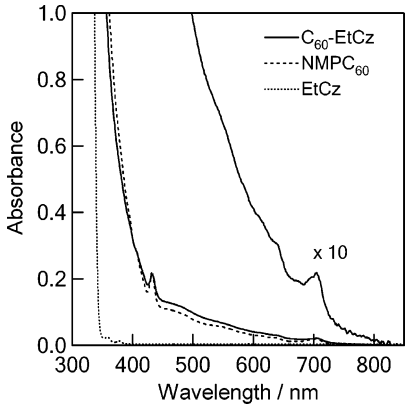

Figure 3. Steady-state absorption spectra of C_{60}−EtCz (0.1 mM) and reference compounds in toluene.

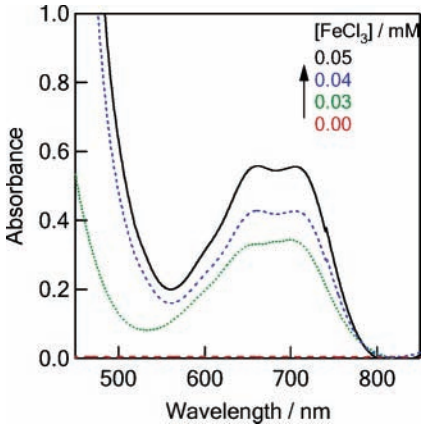

Figure 4. Steady-state absorption spectra of 0.05 mM EtCz (red) in the presence of $FeCl_3$ in PhCN.

Electrochemical Studies. The electrochemical properties of C_{60}−EtCz, C_{60}−TPA, and C_{60}−TPA(Me) have been studied by cyclic voltammetry measurements in benzonitrile (PhCN) and dimethylformamide (DMF). The first negative potentials are attributed to the E_{red} values of the C_{60} moiety, and the first positive potential is assigned to the E_{ox} value of the EtCz or TPA moiety by comparing the E_{red} and E_{ox} values of reference compounds in PhCN and DMF. These E_{red} and E_{ox} values are listed in Table 1. Comparison of these values for dyads with those of reference compounds confirms that there is no appreciable electronic interaction between the C_{60} moiety and the EtCz or TPA moieties in the ground state. In the case of DMF, however, the E_{red} values of the C_{60} moiety shifted to a less negative direction by ca. 0.1 V compared with that in PhCN; this shift may be one of the interesting behaviors of the C_{60}−donor molecules in highly polar DMF.

The energy levels (ΔG_{RIP}) of the radical ion pairs ($C_{60}^{\bullet-}$−$EtCz^{\bullet+}$, $C_{60}^{\bullet-}$−$TPA^{\bullet+}$, and $C_{60}^{\bullet-}$−$TPA(Me)^{\bullet+}$), which are equal to the free-energy changes of charge recombination (ΔG_{CR}), were evaluated as a difference between the E_{ox} and E_{red} values, considering the Coulomb energy (ΔG_S) by the Weller equations (eqs 1 and 2).[30] The free-energy changes for charge separation (ΔG_{CS}) can be calculated by considering the energy levels of the lowest excited state of the C_{60} moiety (ΔE_{0-0}), when the C_{60} moiety was selectively excited.

$$\Delta G_{RIP} = -\Delta G_{CR} = -E_{ox} + E_{red} - \Delta G_S \quad (1)$$

$$-\Delta G_{CS} = \Delta E_{0-0} - \Delta G_{RIP} \quad (2)$$

The calculated ΔG_{CR}, ΔG^S_{CS} (CS via $^1C_{60}$*), and ΔG^T_{CS} (CS via $^3C_{60}$*) values are listed in Tables 2 and 3.

Steady-State Absorption Measurements. Figure 3 shows steady-state absorption spectra of C_{60}−EtCz, $NMPC_{60}$, and EtCz in toluene. The C_{60} moiety of C_{60}−EtCz shows the absorption bands at 705 nm, 435 nm, and shorter than 400 nm,[26] while the EtCz moiety shows the absorption shorter than 350 nm. No additional absorption band or no appreciable shift was observed for C_{60}−EtCz compared with the sum of the absorptions of $NMPC_{60}$ and EtCz. This finding suggests that there is no strong interaction in the ground state between the C_{60} moiety and EtCz moiety in C_{60}−EtCz. Similar results were obtained in PhCN and DMF. Furthermore, for the absorption spectra of C_{60}−TPA and C_{60}−TPA(Me), no spectral change was observed suggesting no appreciable interaction in the ground state between the C_{60} and TPA or TPA(Me) moieties. In the fluorescence and transient absorption measurements, the selective excitation of the C_{60} moiety in C_{60}−EtCz, C_{60}−TPA, and C_{60}−TPA(Me) was possible with light longer than 400 nm.

On addition of $FeCl_3$ to EtCz in PhCN, new broad absorption bands appeared in the visible region around 660−710 nm (Figure 4), which can be attributed to the cation radical of EtCz ($EtCz^{\bullet+}$).[31] From the amount of added $FeCl_3$, the extinction coefficient ($\epsilon_{710\,nm}$) of the absorption peak of $EtCz^{\bullet+}$ was evaluated as about 9300 M^{-1} cm^{-1}. The absorption at 710 nm was similarly observed for C_{60}−EtCz by the chemical oxidation with $FeCl_3$ in PhCN; the $\epsilon_{710\,nm}$ value was the same within experimental error.

Steady-State Fluorescence Measurements. Figure 5a shows the steady-state fluorescence spectra of C_{60}−EtCz measured with the excitation at 520 nm in toluene and DMF. The fluorescence peak at 715 nm is attributed to that of the C_{60} moiety in C_{60}−EtCz by comparing it with the fluorescence peak of $NMPC_{60}$.[26] By comparing the fluorescence peak and the absorption peak (705 nm), it was revealed that $^1C_{60}$*−EtCz shows a small Stokes shift and has the lowest singlet excited energy at 1.75 eV.[26] The fluorescence intensity of $^1C_{60}$*−EtCz in toluene was almost the same as that of $NMPC_{60}$, while the fluorescence intensities of $^1C_{60}$*−EtCz decrease with solvent polarity; i.e., the peak intensity decreased by a factor of 1/3 in DMF with broadening of the fluorescence band by comparing with that in toluene. These observations suggest that some parts of $^1C_{60}$*−EtCz induce the CS process generating $C_{60}^{\bullet-}$−$EtCz^{\bullet+}$ by excitation with 520 nm light. For C_{60}−TPA and C_{60}−TPA(Me), similar solvent polarity effects on the fluorescence spectra were

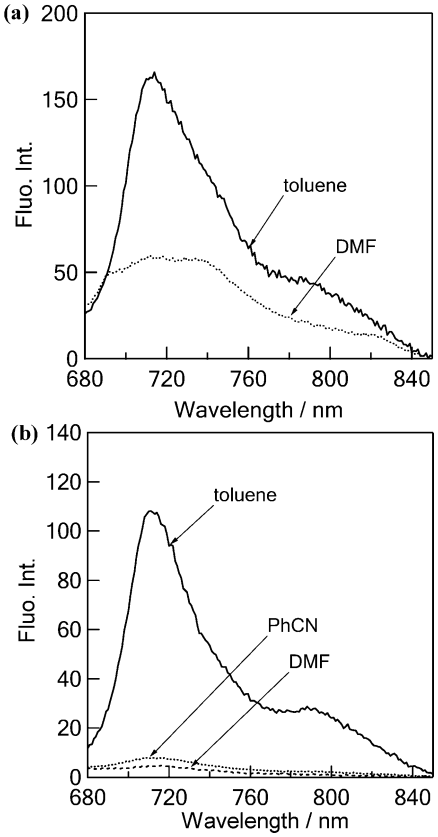

Figure 5. Steady-state fluorescence spectra of (a) C_{60}−EtCz (0.1 mM) in toluene and DMF and (b) C_{60}−TPA(Me) in DMF, PhCN, and toluene; $\lambda_{ex} = 520$ nm.

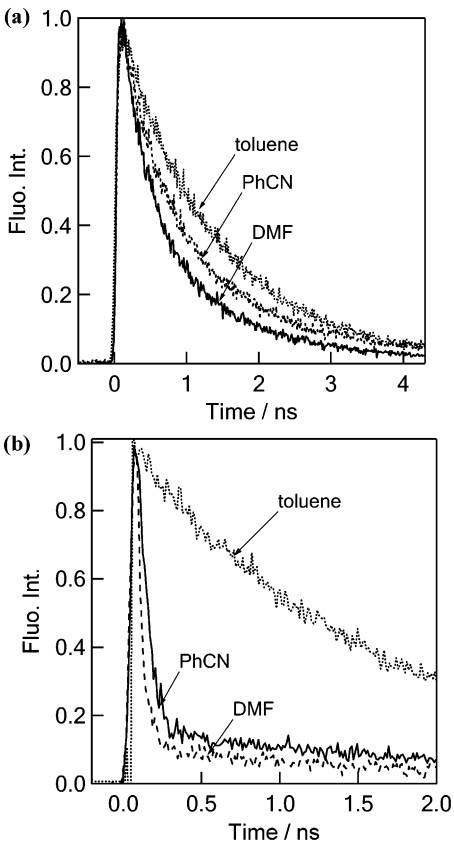

Figure 6. Fluorescence decay profiles around 700−800 nm of (a) C_{60}−EtCz and (b) C_{60}−TPA(Me) in toluene, PhCN, and DMF after 410 nm laser irradiation.

observed; however, the fluorescence intensities of C_{60}−TPA and C_{60}−TPA(Me) in polar solvents were significantly lower than that in toluene as shown in Figure 5b. These observations suggest that CS predominantly takes place from the excited singlet state of the C_{60} moiety in C_{60}−TPA and C_{60}−TPA(Me). On the other hand, some parts of $^1C_{60}$*−EtCz deactivated via intersystem crossing (ISC) to $^3C_{60}$*−EtCz.

Fluorescence Lifetime Measurements. The fluorescence lifetimes (τ_f) of C_{60}−EtCz, C_{60}−TPA, C_{60}−TPA(Me), and $NMPC_{60}$ were measured using a time-correlated single-photon-counting apparatus with excitation at 410 nm. As shown in Figure 6a, fluorescence time profile of $^1C_{60}$*−EtCz at 700−800 nm in toluene shows single-exponential decay, giving a τ_f value. In toluene, the τ_f value of $^1C_{60}$*−EtCz was estimated to be 1400 ps, which is nearly equal to that of $NMPC_{60}$ (1300 ps), suggesting that only intersystem crossing takes place without charge separation.[13] In PhCN and DMF, fluorescence time profiles of $^1C_{60}$*−EtCz at 700−800 nm showed two component exponential decays, giving two τ_f values. From the initial fast decay parts of $^1C_{60}$*−EtCz, the τ_f values were evaluated to be 715 ps as a fraction of 79% in PhCN and 480 ps as a fraction of 73% in DMF. On the other hand, the CS processes of C_{60}−TPA and C_{60}−TPA(Me) via the$^1C_{60}$* moiety were suggested by the rapid decays of the fluorescence time profiles in polar solvents as shown in Figure 6b. Each time profile shows biexponential decay in DMF and PhCN; the τ_f values of the $^1C_{60}$* moieties in C_{60}−TPA and C_{60}−TPA(Me) were evaluated to be shorter than 130 ps from the major initial decay. For $^1C_{60}$*−TPA and $^1C_{60}$*−TPA(Me), these τ_f values are considerably shorter than those of $^1C_{60}$*−EtCz.

The rate constant (k^S_{CS}) and the quantum yield (Φ^S_{CS}) for the CS processes via $^1C_{60}$*−EtCz and $^1C_{60}$*−TPAs were calculated by eqs 3 and 4, where the $(\tau_f)_{sample}$ and $(\tau_f)_{ref}$ refer to the fluorescence lifetimes of sample and reference ($NMPC_{60}$), respectively.[9b,10c,11]

$$k^S_{CS} = (1/\tau_f)_{sample} - (1/\tau_f)_{ref} \quad (3)$$

$$\Phi^S_{CS} = [(1/\tau_f)_{sample} - (1/\tau_f)_{ref}]/(1/\tau)_{sample} \quad (4)$$

These k^S_{CS} and Φ^S_{CS} values are listed in Table 2. The k^S_{CS} values increase in the order of C_{60}−EtCz ≪ C_{60}−TPA < C_{60}−TPA(Me). The Φ^S_{CS} values of C_{60}−TPA and C_{60}−TPA(Me) are greater than 0.9 in PhCN and DMF, suggesting that the CS process predominantly takes place via the $^1C_{60}$* moiety, while the Φ^S_{CS} values of C_{60}−EtCz are less than 0.66, indicating that the remaining part of the $^1C_{60}$* moiety may transfer to the $^3C_{60}$* moiety via ISC. Furthermore, by comparing with C_{60}−TPA, the CS process for C_{60}−TPA(Me) is rapid and efficient in polar solvents, indicating that the CH_3-substituted TPA enhances the donor ability. These findings afford a guideline to design new short linkage C_{60}−donor dyads with an efficient CS process via the $^1C_{60}$* moiety.

Time-Resolved Transient Absorption Spectra. A transient absorption spectrum of C_{60}−EtCz observed in toluene by nanosecond laser light excitation at 532 nm showed a peak at 700 nm, which was attributed to the $^3C_{60}$* moiety in C_{60}−EtCz (Figure 7).[25−27] In PhCN, a similar spectrum was obtained for C_{60}−EtCz, although the intensity was weak. The transient spectrum of C_{60}−TPA(Me) in PhCN is also shown in Figure 7; although the intensity is weak, the shape of the spectrum is the same as that of the $^3C_{60}$* moiety. In Figure 7, the appearance of the absorption band at 1000 nm due to the $C_{60}^{\bullet-}$ moiety was

TABLE 2: Fluorescence Lifetime (τ_f at 700−750 nm), Charge Separation Rate Constant (k^S_{CS}), Quantum Yield for Charge Separation (Φ^S_{CS}) via $^1C_{60}$*, and Free-Energy Change of Charge Separation (ΔG_{CS}) of C_{60}−EtCz, C_{60}−TPA, and C_{60}−TPA(Me) in Toluene, PhCN, and DMF

compound	solvent	τ_f[a]/ps	k^S_{CS}[b]/s^{-1}	Φ^S_{CS}[b]	$-\Delta G^S_{CS}$[c]/eV	$-\Delta G^T_{CS}$[c]/eV
C_{60}−EtCz	toluene	1400 (100%)		0	−0.23	−0.48
	PhCN	715 (79%)	6.9×10^8	0.49	0.29	0.04
	DMF	480 (73%)	1.4×10^9	0.66	0.50	0.25
C_{60}−TPA	toluene	1380 (100%)		0	−0.40	−0.65
	PhCN	130 (96%)	7.3×10^9	0.91	0.22	−0.03
	DMF	100 (81%)	9.1×10^9	0.93	0.38	0.13
C_{60}−TPA(Me)	toluene	1400 (100%)		0	−0.13	−0.38
	PhCN	88 (90%)	1.1×10^{10}	0.94	0.33	0.09
	DMF	58 (93%)	1.7×10^{10}	0.96	0.46	0.21

[a] Shorter fluorescence lifetimes. [b] Calculated by eqs 3 and 4, $(\tau_f)_{ref}$ was 1480 ps for NMPC$_{60}$ in toluene. k_{CS} and Φ_{CS} were calculated from the shorter lifetimes. [c] ΔG_{CS} was calculated from eqs 1 and 2. In PhCN and DMF, $\Delta G_S = e^2/\{(4\pi\epsilon_0)\epsilon_s R_{cc}\}$. In toluene, $\Delta G_S = e^2/\{(4\pi\epsilon_0)[(1/(2R_+) + 1/(2R_-) - 1/R_{cc})/\epsilon_s - (1/(2R_+) + 1/(2R_-))/\epsilon_R]\}$, where R_+ and R_- are cation and anion radii, which were evaluated from the HOMO and LUMO, respectively. ϵ_s and ϵ_R are dielectric constants of solvents used for measuring the redox potentials.[30]

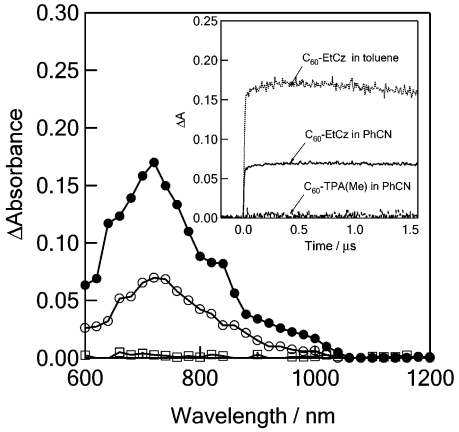

Figure 7. Nanosecond transient absorption spectra of C_{60}−EtCz (0.1 mM) and C_{60}−TPA(Me) observed by 532 nm laser irradiation after 100 ns; C_{60}−EtCz in toluene (●) and PhCN (○) and C_{60}−TPA(Me) in PhCN (□). Inset: absorption−time profiles at 720 nm in toluene and PhCN.

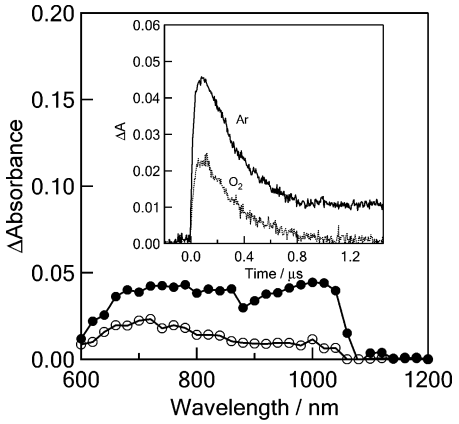

Figure 8. Nanosecond transient absorption spectra of C_{60}−EtCz (0.1 mM) observed by 532 nm laser irradiation at 0.1 (●) and 1.0 μs (○) in DMF. Inset: absorption−time profiles at 1000 nm in Ar and O_2-saturated DMF.

not observed; the absorption from 900 to 1050 nm can be attributed to the absorption tail of the $^3C_{60}$* moiety.

In the transient spectra of C_{60}−EtCz in DMF at 0.1 μs (Figure 8), on the other hand, the transient absorption bands appeared around 1000 nm, which is attributed to the $C_{60}^{\bullet-}$ moiety.[28] The broad absorption bands in the visible region around 620 and 780 nm were assigned to the $EtCz^{\bullet+}$ moiety in C_{60}−EtCz. Since the ratio of the extinction coefficient around 710 nm of the $EtCz^{\bullet+}$ moiety to that of the $C_{60}^{\bullet-}$ moiety at 1000 nm is ca. 1, it is confirmed that the transient spectrum in DMF exclusively results from $C_{60}^{\bullet-}$−$EtCz^{\bullet+}$.

For C_{60}−TPA and C_{60}−TPA(Me), a drastic decrease of the absorption intensity of the $^3C_{60}$* moiety was observed in PhCN and DMF, suggesting that the quick rise and quick decay occur within 6 ns, which was our instrument limit.[27] However, by the comparison of the absorption intensity of the $^3C_{60}$* moiety generated by one shot of the laser light in toluene, the relative quantum yield for the $^3C_{60}$* generation (Φ_T^{obs}) was observed as a standard in toluene ($\Phi_T^{obs} = 1$), as listed in Table 3. These Φ_T^{obs} values are in the good agreement with the Φ_T^{calc} values calculated from Φ^S_{CS} ($\Phi_T^{calc} = 1 - \Phi^S_{CS}$). This supports that the quick CS and quick CR processes are hidden in the transient spectra in Figure 7. Furthermore, the good agreement of the Φ_T^{obs} values with the Φ_T^{calc} values suggests that the CS process via $^3C_{60}$* is not possible in toluene, PhCN, and DMF, excepting C_{60}−EtCz in DMF. Thermodynamically, this process for C_{60}−EtCz is supported, because the ΔG^T_{CS} values are positive in toluene and almost zero in PhCN. In DMF, on the other hand, generation of the $^3C_{60}$* moiety was kinetically prohibited for C_{60}−TPA and C_{60}−TPA(Me), although sufficiently negative ΔG^T_{CS} values thermodynamically permit the CS process via the $^3C_{60}$* moiety.

The time profile (Figure 8) at 1000 nm in DMF shows appreciable decay of $C_{60}^{\bullet-}$−$EtCz^{\bullet+}$ in the time region until 500 ns, which obeys first-order kinetics with a rate constant of 3.4×10^6 s^{-1} at room temperature. This decay process is attributed to the CR process (k_{CR}) of $C_{60}^{\bullet-}$−$EtCz^{\bullet+}$ in DMF; thus, from the inverse of the k_{CR} values, the lifetime (τ_{RIP}) of the radical ion pair ($C_{60}^{\bullet-}$−$EtCz^{\bullet+}$) was evaluated to be 300 ns in DMF at room temperature. This τ_{RIP} value is significantly longer than those of $C_{60}^{\bullet-}$−$TPA^{\bullet+}$ or $C_{60}^{\bullet-}$−$TPA(Me)^{\bullet+}$.

In further longer time scale measurements for $C_{60}^{\bullet-}$−$EtCz^{\bullet+}$ in DMF, the absorption seems to persist until 100 μs, which may be attributed to the absorption tail of the $^3C_{60}$* moiety with long lifetimes.[26−28] It is notable that, on the addition of O_2, this long-lived tail of the 1000 nm band completely decayed within 500 ns, which supports that the long-lived absorption tail of the $^3C_{60}$* moiety is overlapping with that of the radical ion pair. The decrease of the absorption intensity at 1000 nm on the addition of O_2 is probably due to the quenching of the $^3C_{60}$* moiety, which is a precursor of the CS process, by O_2. In addition, the decay of $C_{60}^{\bullet-}$−$EtCz^{\bullet+}$ was accelerated by the addition of O_2; the decay rate constant of $C_{60}^{\bullet-}$−$EtCz^{\bullet+}$ was evaluated to be 4.1×10^6 s^{-1}. On assuming $[O_2] = 5$ mM in O_2-saturated DMF, the bimolecular rate constant was estimated to be 8×10^9 M^{-1} s^{-1}, which is close to diffusion-controlled limit in DMF. This observation suggests that $C_{60}^{\bullet-}$−$EtCz^{\bullet+}$ has

TABLE 3: Quantum Yield (Φ_T) for Generation of $^3C_{60}$*, Lifetime (τ_{RIP}) of Radical Ion Pair, and Charge Recombination Free Energy ($-\Delta G_{CR}$) of C_{60}−EtCz, C_{60}−TPA, and C_{60}−TPA(Me) in Toluene, PhCN and DMF

compound	solvent	Φ_T^{calc} [a]	Φ_T^{obs} [b]	τ_{RIP}/ns	$-\Delta G_{CR}$ [c]/eV
C_{60}−EtCz	toluene	1.00	(1)		1.98
	PhCN	0.51	0.40	<6	1.46
	DMF	0.34	d	300	1.25
C_{60}−TPA	toluene	1.00	(1)		2.15
	PhCN	0.09	0.09	<6	1.55
	DMF	0.07	0.06	<6	1.37
C_{60}−TPA(Me)	toluene	1.00	(1)		1.88
	PhCN	0.06	0.05	<6	1.42
	DMF	0.04	0.04	<6	1.29

[a] $\Phi_T^{calc} = 1 - \Phi^S_{CS}$. [b] From the transient absorbance at 720 nm. [c] ΔG_{CR} was calculated from eq 1; details are shown in footnote *c* of Table 2. [d] Due to the overlap of the absorption of $EtCz^{+\bullet}$, Φ_T^{obs} cannot be observed.

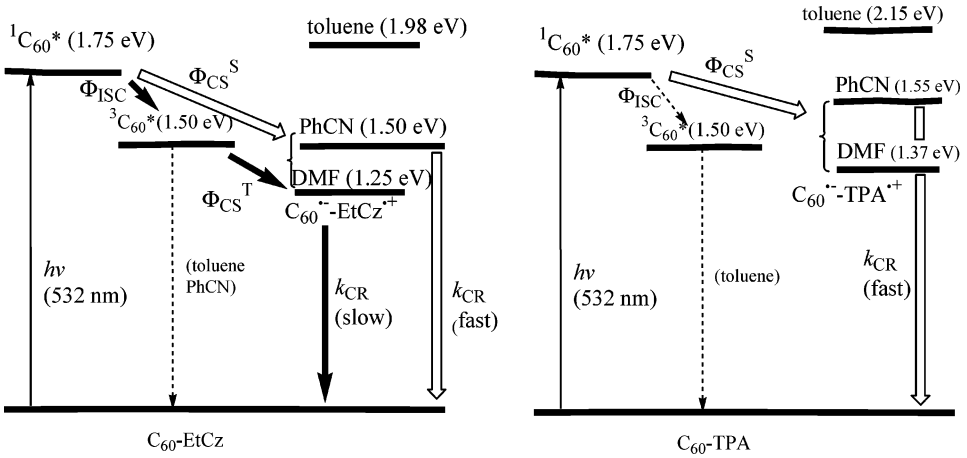

Figure 9. Schematic energy diagrams and excitation energy and electron flows of C_{60}−EtCz and C_{60}−TPA.

triplet spin character, since the reaction of $C_{60}^{\bullet-}$ and O_2 is considered to be slow.[10c]

Energy Diagrams. From the ΔG_{CR} and ΔG_{CS} values and the energy levels of the lowest excited states, energy diagrams for C_{60}−EtCz and C_{60}−TPAs can be illustrated. In Figure 9, the reported E_{0-0} values of the $^1C_{60}$* and $^3C_{60}$* moieties, 1.75 and 1.50 eV, respectively, were employed. The energy levels of $C_{60}^{\bullet-}$−EtCz$^{\bullet+}$ and $C_{60}^{\bullet-}$−TPA$^{\bullet+}$ depend on the solvent polarity. Therefore, since the energy levels of $C_{60}^{\bullet-}$−EtCz$^{\bullet+}$ and $C_{60}^{\bullet-}$−TPA$^{\bullet+}$ in toluene are higher than that of the $^1C_{60}$* state, no CS process via $^1C_{60}$* takes place, resulting in the predominant observation of $^3C_{60}$* with long lifetime.[26] In PhCN and DMF, the CS process via $^1C_{60}$* is possible. In DMF, the CS process via $^3C_{60}$* is also thermodynamically possible. However, by kinetic reasoning, this process is only possible for C_{60}−EtCz in DMF.

In the CR process, the τ_{RIP} value of $C_{60}^{\bullet-}$−EtCz$^{\bullet+}$ in DMF was exceptionally long, while it is short in PhCN, which cannot be explained by the Marcus inverted region,[32] because the absolute value of ΔG_{CR} in DMF (1.25 eV) is smaller than that in PhCN (1.46 eV), although these values are smaller than the reported reorganization energy (ca. 0.7 eV).[9] Rather, it is considered that the spin character of $C_{60}^{\bullet-}$−EtCz$^{\bullet+}$, which reflects the triplet state of the precursor, is responsible for the long-lived CS state.

Comparison with Other Dyads and Triads. The τ_{RIP} value for a dyad composed of C_{60}−(fluorene−diphenylamine) was evaluated to be 150 ns in DMF at room temperature.[25a] Comparing with the reported τ_{RIP} values for the covalently connected dyads, i.e., C_{60}−biphenylamine dyad (220 ns),[13a] the τ_{RIP} value of the radical ion pair ($C_{60}^{\bullet-}$−EtCz$^{\bullet+}$) in DMF is longer. In the case of C_{60}−bridge−dimethylaniline systems, τ_{RIP} values in the range of 8−250 ns were reported, depending on the kinds and lengths of the bridge molecules.[11] Compared with these C_{60} and amine dyads, $C_{60}^{\bullet-}$−EtCz$^{\bullet+}$ in DMF showed a long τ_{RIP} value, even using simple bridges. Recently, for C_{60}−triphenylamine dyad with a benzothiadiazole bridge, relatively longer lifetimes have been reported only in DMF, suggesting that DMF has specially favorable properties for the charge-separated state.[13b]

Conclusions

For C_{60} covalently linked to TPA and TPA(Me), the photoinduced CS process takes place predominantly via the $^1C_{60}$* moiety producing CS states ($C_{60}^{\bullet-}$−TPA$^{\bullet+}$ and $C_{60}^{\bullet-}$−TPA(Me)$^{\bullet+}$) in polar solvents. For C_{60}−EtCz, on the other hand, the CS process takes place via the $^3C_{60}$* moiety, in addition to via the $^1C_{60}$* moiety in DMF. A prolonged lifetime of $C_{60}^{\bullet-}$−EtCz$^{\bullet+}$ in DMF was observed, probably due to the triplet spin character of $C_{60}^{\bullet-}$−EtCz$^{\bullet+}$ generated via the $^3C_{60}$* moiety. On the other hand, the CS states generated via the $^1C_{60}$* moiety have short lifetimes. These findings afford a guideline to design new short linkage C_{60}−donor dyads with efficient CS states via the $^1C_{60}$* and $^3C_{60}$* moieties, giving long charge-separated states.

Experimental Section

Reagents. C_{60} (purity >99.9%) was purchased from 3D Carbon Cluster Material Co. of Wuhan University in China; the corresponding starting materials and solvents were purchased from Tokyo Casei Inc. All solvents for electrochemical and spectral measurements were spectroscopic or HPLC grade.

General. All melting points are uncorrected. IR spectra were recorded on a Perkin-Elmer Fourier transform infrared spectrometer and measured as KBr pellets or Nujol. ^{1}H NMR spectra

were determined in $CDCl_3$ or $CDCl_3/CS_2$ with a Varian INOVA 500 MHz spectrometer. Chemical shifts (δ) are given relative to tetramethylsilane (TMS). The coupling constants (J) are reported in Hz. Elemental analyses were performed with a Perkin-Elmer 2400 analyzer. ESI-MS spectra were recorded with a LCQ DECA XP mass spectrometer at 70 eV using a direct inlet system. Analytical TLC was carried out on silica gel coated on aluminum foil (Merck 60 F_{254}). Column chromatography was carried out on silica gel (Wako C-300). $NMPC_{60}$ was prepared according to methods reported previously.[29]

Synthesis of C_{60}−EtCz. In 100 mL of dry toluene under nitrogen atmosphere, 216 mg (0.3 mmol) of C_{60}, 53.4 mg (0.6 mmol) of sarcosine, and 270 mg (1.2 mmol) of *N*-ethylcarbazole-3-carboxaldehyde were dissolved. After microwave irradiation for 2 h, the brown solution was concentrated and the raw solid product was purified by flash column chromatography on silica gel (100−200 mesh) to give monocycloadduct (54.2 mg, 18.62%). $R_f = 0.33$ (toluene/petroleum ether = 2:3). FT-IR (KBr) ν (cm^{-1}): 2921.59, 2850.59, 2769.23, 1629.37, 1461.00, 1382.74, 1330.61, 1262.03, 1231.85, 1121.14, 801.15, 743.53, 525.92. ^1H NMR ($CS_2/CDCl_3$) δ: 7.435−7.017 (m, 8H, ArH), 5.095 (s, 1H), 5.02 (d,1H, $J = 9.75$ Hz), 4.34 (q, 2H, $J = 7$ Hz), 4.31 (d, 1H, $J = 9.75$ Hz), 2.84 (s, 3H, NCH_3), 1.46 (t, 3H, $J = 7$ Hz). ESI-MS m/z ($M + H^+$): 971. Anal. Calcd for $C_{77}H_{18}N_2$: C, 95.26%; H, 1.86%; N, 2.89%. Found: C, 94.96%; H, 1.93%; N, 2.78%.

Synthesis of C_{60}−TPA. In general, 216 mg (0.3 mmol) of C_{60}, 53.4 mg (0.6 mmol) of sarcosine, and 328 mg (1.2 mmol) of 4-(*N*,*N*-diphenylamino)benzaldehyde were dissolved in 100 mL of dry toluene under nitrogen atmosphere. After microwave irradiation for 2 h, the brown solution was concentrated and the raw solid product was purified by flash column chromatography on silica gel (100−200 mesh) to give monocycloadduct (29.8 mg, 9.74%). $R_f = 0.51$ (toluene/petroleum ether = 2:3). FT-IR (KBr) ν (cm^{-1}): 2921.92., 2846.15, 2357.14, 1623.43, 1459.74, 1382.74, 1273.00, 1119.38, 614.60, 526.81. ^1H NMR ($CDCl_3$:CS_2) δ: 7.27−6.95 (m, 14H, ArH), 4.98 (d, 1H, $J_{AB} = 9$ Hz), 4.92 (s, 1H), 4.29 (d, 1H, $J_{AB} = 9$ Hz), 2.88 (s, 3H, NCH_3). ESI-MS m/z ($M + H^+$): 1021. Anal. Calcd for $C_{81}H_{20}N_2$: C, 95.29%; H, 1.96%; N, 2.75%. Found: C, 95.14%; H, 2.00%; N, 2.72%.

Synthesis of C_{60}−TPA(Me). In 100 mL of dry toluene under nitrogen atmosphere, 216 mg (0.3 mmol) of C_{60}, 53.4 mg (0.6 mmol) of sarcosine, and 360 mg (1.2 mmol) of 4-(di-*p*-tolylamino)benzaldehyde were dissolved. After microwave irradiation for 2 h, the brown solution was concentrated and the raw solid product was purified by flash column chromatography on silica gel (100−200 mesh) to give monocycloadduct (32.3 mg, 10.24%). $R_f = 0.41$ (toluene/petroleum ether = 2:3). FT-IR(KBr) ν (cm^{-1}): 2919.26, 2846.15, 2774.72, 2351.64, 1629.49, 1504.80, 1382.74, 1271.11, 1121.45, 809.38, 724.33, 526.24 ^1H NMR ($CS_2/CDCl_3$) δ: 7.23−6.85 (m, 12H, ArH), 4.94 (d, 1H, $J_{AB} = 9.25$ Hz), 4.85 (s, 1H), 4.24−4.22 (d, 1H, $J_{AB} = 9.25$ Hz), 2.824 (s, 3H, NCH_3), 1.387 (s, 3H, CH_3). ESI-MS m/z ($M + H^+$): 1049. Anal. Calcd for $C_{83}H_{24}N_2$: C, 95.04%; H, 2.29%; N, 2.67%. Found: C, 94.65%; H, 2.55%; N, 2.45%.

Spectral Measurements. Time-resolved fluorescence spectra were measured by a single-photon-counting method using the second harmonic generation (SHG, 410 nm) of a Ti:sapphire laser [Spectra Physics, Tsunami 3950-L2S, 1.5 ps full width at half-maximum (fwhm)] and a streak scope (Hamamatsu Photonics, C4334-01) equipped with a polychromator (Action Research, SpectraPro 150) as an excitation source and a detector, respectively.[33]

Nanosecond transient absorption measurements were carried out using the SHG (532 nm) of a Nd:YAG laser (Spectra Physics, Quanta-Ray GCR-130, fwhm 6 ns) as an excitation source. For transient absorption spectra in the near-IR region (600−1600 nm), the monitoring light from a pulsed Xe lamp was detected with a Ge-avalanche photodiode (Hamamatsu Photonics, B2834). Photoinduced events in micro- and millisecond time regions were estimated by using a continuous Xe lamp (150 W) and an InGaAs-PIN photodiode (Hamamatsu Photonics, G5125-10) as a probe light and a detector, respectively. Details of the transient absorption measurements were described elsewhere.[33] All the samples in a quartz cell (1×1 cm) were deaerated by bubbling argon through the solution for 15 min. Steady-state absorption spectra in the visible and near-IR regions were measured on a JACSO V570 DS spectrometer. Fluorescence spectra were measured on a Shimadzu RF-5300PC spectrofluorophotometer.

Electrochemical Measurements. The cyclic voltammetry measurements were performed on a BAS CV-50 W electrochemical analyzer in deaerated PhCN or DMF solution (0.1 mM) containing 0.1 M tetra-*n*-butylammonium perchlorate as a supporting electrolyte at 298 K (100 mV s^{-1}). The glassy carbon working electrode was polished with BAS polishing alumina suspension and rinsed with acetone before use. The counter electrode was a platinum wire. The measured potentials were recorded with respect to an Ag/AgCl (saturated KCl) reference electrode and Fc/Fc^+ was used as an internal standard.

Molecular Orbital Calculations. All calculations were performed by semiempirical PM3 and density functional B3LYP/3-21G(*) method with Gaussian 98 package. The graphics of HOMO and LUMO coefficients were generated with the help of Gauss View software.

Acknowledgment. The authors acknowledge financial support from the National Natural Science Foundation of China (Nos. 20231020, 20471020) and from a Grant-in-Aid for Scientific Research on Priority Area (417) from the Ministry of Education, Science, Sports and Culture of Japan.

References and Notes

(1) (a) Foote, C. S. In *Photophysical and Photochemical Properties of Fullerenes*; Matty, J., Ed.; Topics in Current Chemistry 169; Springer-Verlag: Berlin, 1994, p 347.

(2) *Fullerene, Chemistry, Physics and Technology*; Kadish, K. M., Ruoff, R. S., Eds.; Wiley-Interscience: New York, 2000.

(3) *Molecular and Supramolecular Photochemistry*; Ramamurthy, V., Schanze, K. S., Eds.; Marcel Dekker: New York, 2001; Vol. 7.

(4) Imahori, H.; Sakata, Y. *Adv. Mater.* **1997**, *9*, 537.

(5) Martín, N.; Sánchez, L.; Illescas, B.; Pérez, I. *Chem. Rev.* **1998**, *98*, 2527.

(6) Echegoyen, L.; Echegoyen, L. E. *Acc. Chem. Res.* **1998**, *31*, 593.

(7) Guldi, D. M.; Prato, M. *Acc. Chem. Res.* **2000**, *33*, 695.

(8) Gust, D.; Moore, T. A.; Moore, A. L. *Acc. Chem. Rec.* **2001**, *34*, 40.

(9) (a) Imahori, H.; Hagiwara, K.; Akiyama, T.; Akoi, M.; Taniguchi, S.; Okada, T.; Shirakawa, M.; Sakata, Y. *Chem. Phys. Lett.* **1996**, *263*, 545. (b) Imahori, H.; El-Khouly, M. E.; Fujitsuka, M.; Ito, O.; Sakata, Y.; Fukuzumi, S. *J. Phys. Chem. A* **2001**, *105*, 325.

(10) (a) Imahori, H.; Cardoso, S.; Tatman, D.; Lin, S.; Noss, L.; Seely, G. R.; Sereno, L.; Silber, C.; Moore, T. A.; Moore, A. L.; Gust, D. *Photochem. Photobiol.* **1995**, *62*, 1009. (b) Gust, D.; Moore, T. A.; Moore, A. L. *Res. Chem. Intermed.* **1997**, *23*, 621. (c) Yamazaki, M.; Araki, Y.; Fujitsuka, M.; Ito, O. *J. Phys. Chem. A* **2001**, *105*, 8615. (d) González, S.; Herranz, M. A.; Illescas, B.; Segura, J. L.; Martín, N. *Synth. Met.* **2001**, *121*, 1131.

(11) (a) Williams, R. M.; Zwier, J. M.; Verhoeven, J. W. *J. Am. Chem. Soc.* **1995**, *117*, 4093. (b) Williams, R. M.; Koeberg, M.; Lawson, J. M.; An, Y.-Z.; Rubin, Y.; Paddon-Row, M. N.; Verhoeven, *J. Org. Chem.* **1996**, *61*, 5055.

(12) (a) Thomas, K. G.; Biju, V.; George, M. V.; Guldi, D. M.; Kamat, P. V. *J. Phys. Chem. A* **1998**, *102*, 5341. (b) Thomas, K. G.; Biju, V.; Guldi, D. M.; Kamat, P. V.; George, M. V. *J. Phys. Chem. A* **1999**, *103*, 10755.

(13) (a) Komamine, S.; Fujitsuka, M.; Ito, O.; Moriwaki, K.; Miyata, T.; Ohno, T. *J. Phys. Chem. A* **2000**, *104*, 11497. (b) Sandanayaka, S. D. A.; Matsukawa, K.; Ishi-I, T.; Mataka, S.; Araki, Y.; Ito, O. *J. Phys. Chem. B* **2004**, *108*, 19995. (c) Sandanayaka, S. D. A.; Sasabe, H.; Araki, Y.; Furusho, Y.; Ito, O.; Takata, T. *J. Phys. Chem. A* **2004**, *108*, 5145.

(14) Yonemura, H.; Moribe, S.; Hayashi, K.; Noda, M.; Tokudome, H.; Yamada, S.; Nakamura, H. *Appl. Magn. Reson.* **2003**, *23*, 289.

(15) (a) Liddell, P. A.; Kuciauskas, D.; Sumida, J. P.; Nash, B.; Nguyen, D.; Moore, A. L.; Moore, T. A.; Gust, D. *J. Am. Chem. Soc*. **1997**, *119*, 1400. (b) Liddell, P. A.; Kodis, G.; Moore, A. L.; Moore, T. A.; Gust, D. *J. Am. Chem. Soc*. **2002**, *124*, 7668.

(16) (a) Imahori, H.; Yamada, K.; Hasegawa, M.; Taniguchi, S.; Okada, T.; Sakata, Y. *Angew. Chem., Int. Ed. Engl*. **1997**, *36*, 2626. (b) Imahori, H.; Tamaki, K.; Araki, Y.; Sekiguchi, Y.; Ito, O.; Sakata, Y.; Fukuzumi, S. *J. Am. Chem. Soc*. **2002**, *124*, 5165.

(17) (a) Linssen, T. G.; Durr, K.; Hannack, M.; Hirsh, A. *J. Chem. Soc., Chem. Commun.* **1995**, 103. (b) Durr, K.; Fiedler, S.; Linssen, T.; Hirshi, A.; Hanack, M. *Chem. Ber*. **1997**, *130*, 1375.

(18) (a) Saster, A.; Gouloumis, A.; Vazques, P.; Torres, T.; Doan, V.; Schwartz, B. J.; Wudl, F.; Echigoyen, L.; Rivera, J. *Org. Lett*. **1999**, *1*, 1807. (b) Martinez-Diaz, M. V.; Fender, N. S.; Rodriguez-Morgade, M. S.; Gomes-Lopes, M.; Dietrich, F.; Echioyen, L.; Stoddart, J. F.; Torres, T. *J. Mater. Chem*. **2002**, *12*, 2095.

(19) (a) Sacricifici, N. S.; Wudl, F.; Heeger, A. J.; Maggini, M.; Scorrano, G.; Prato, M.; Bourassa, J.; Ford, P. C. *Chem. Phys. Lett*. **1995**, *247*, 210. (b) Maggini, M.; Dono, A.; Scorrano, G.; Prato, M. *J. Chem. Soc., Chem. Commun*. **1998**, 845. (c) Guldi, D. M.; Maggini, M.; Scorrano, G.; Prato, M. *J. Am. Chem. Soc*. **1997**, *119*, 974.

(20) (a) D'Souza, F.; Zandler, M. E.; Smith, P. M.; Deviprasad, G. R.; Arkady, K.; Fujitsuka, M.; Ito, O. *J. Phys. Chem. A* **2002**, *106*, 649. (b) Fujitsuka, N.; Tsuboya, R.; Hamasaki, M.; Ito, S.; Onodera, S.; Ito, O.; Yamamoto, Y. *J. Phys. Chem. A* **2003**, *107*, 1452.

(21) (a) Martín, N.; Sánchez, L.; Herranz, M. A.; Guldi, D. M. *J. Phys. Chem. A* **2000**, *104*, 4648. (b) Sánchez, L.; Pérez, I.; Martín, N.; Guldi, D. M. *Chem. Eur. J.* **2003**, *9*, 2457.

(22) (a) Allard, E.; Cousseau, J.; Oruduna, J.; Garin, J.; Luo; H.; Araki, Y.; Ito, O. *Phys. Chem. Chem. Phys.* **2002**, *4*, 5944. (b) Kreher, D.; Hudhomme, P.; Gorgues, A.; Luo, H.; Araki, Y.; Ito, O. *Phys. Chem. Chem. Phys.* **2003**, *5*, 4583.

(23) (a) Yamashiro, T.; Aso, Y.; Otsubo, T.; Tang, H.; Harima, T.; Yamashita, K. *Chem. Lett.* **1999**, 443. (b) Fujitsuka, M.; Ito, O.; Yamashiro, T.; Aso, Y.; Otsubo, T. *J. Phys. Chem. A* **2000**, *104*, 4876. (c) Fujitsuka, M.; Matsumoto, K.; Ito, O.; Yamashiro, T.; Aso, Y.; Otsubo, T. *Res. Chem. Intermed*. **2001**, *27*, 73.

(24) (a) van Hal, P. A.; Knol, J.; Langeveld-Voss, B. M. W.; Meskers, S. C. J.; Hummelen, J. C.; Janssen, R. A. J. *J. Phys. Chem. A* **2000**, *104*, 5974. (b) Beckers, E. H. A.; van Hal, P. A.; Dhanabalan, A.; Meskers, S. C. J.; Knol, J.; Hummelen, J. C.; Janssen, R. A. J. *J. Phys. Chem. A* **2003**, *107*, 6218.

(25) (a) Luo, H.; Fujitsuka, M.; Araki, Y.; Ito, O.; Padmawar, P.; Chiang, L. Y. *J. Phys. Chem. B* **2003**, *107*, 9312. (b) Yamanaka, K.; Fujitsuka, M.; Araki, Y.; Ito, O.; Aoshima, T.; Fukushima, T.; Miyashi, T. *J. Phys. Chem. A* **2004**, *108*, 250.

(26) (a) Arbogast, J. W.; Foote, C. S.; Kao, M. *J. Am. Chem. Soc*. **1992**, *114*, 2277. (b) Steren, C. A.; von Willigen, H.; Biczok, L.; Gupta, N.; Linschitz, H. *J. Phys. Chem*. **1996**, *100*, 8920.

(27) (a) Komamine, S.; Fujitsuka, M.; Ito, O.; Itaya, A. *J. Photochem. Photobiol. A: Chem*. **2000**, *135*, 111. (b) Yahata, Y.; Sasaki, Y.; Fujitsuka, M.; Ito, O. *J. Photosci.* **1999**, *6*, 117.

(28) (a) Sension, R. J.; Szarka, A. Z.; Smith, G. R.; Hochstrasser, R. M. *Chem. Phys. Lett*. **1991**, *185*, 179. (b) Ghosh, H. N.; Palit, D. K.; Sapre, A. V.; Mittal, J. P. *Chem. Phys. Lett*. **1997**, *265*, 365.

(29) Maggini, M.; Scorrano, G.; Prato, M. *J. Am. Chem. Soc*. **1993**, *115*, 9798.

(30) Weller, A. *Z. Phys. Chem., Neue Folge* **1982**, *133*, 93.

(31) *Electronic Absorption Spectra of Radical Ions*; Shida, T., Ed.; Elsevier Science Publishing Company: Amsterdam, The Netherlands, 1988; p 212.

(32) Marcus, R. A.; Sutin, N. *Biochim. Biophys. Acta* **1985**, *811*, 265.

(33) (a) Watanabe, N.; Kihara, N.; Furusho, Y.; Takata, T.; Araki, Y.; Ito, O. *Angew. Chem., Int. Ed.* **2003**, *42*, 681. (b) Choi, M. S.; Aida, T.; Luo, H.; Araki, Y.; Ito, O. *Angew. Chem., Int. Ed.* **2003**, *42*, 4060. (c) Makinoshima, T.; Fujitsuka, M.; Sasaki, M.; Araki, Y.; Ito, O.; Ito, S.; Morita, N. *J. Phys. Chem. A* **2004**, *108*, 368.